SUPER–RESOLVED TIME–OF–FLIGHT SENSING VIA FRI SAMPLING THEORY

Ayush Bhandari[*], *Andrew M. Wallace*[◇] *and Ramesh Raskar*[*]

[*]Media Laboratory, Massachusetts Institute of Technology, Cambridge, MA, USA.
[◇]School of Engineering and Physical Sciences, Heriot–Watt University, Edinburgh, Scotland.
Email: ayush@MIT.edu • A.M.Wallace@hw.ac.uk • raskar@MIT.edu

ABSTRACT

Optical time–of–flight (ToF) sensors can measure scene depth accurately by projection and reception of an optical signal. The range to a surface in the path of the emitted signal is proportional to the delay time of the light echo or the reflected signal. In practice, a diverging beam may be subject to multi-echo backscatter, and all these echoes must be resolved to estimate the multiple depths. In this paper, we propose a method for super-resolution of optical ToF signals. Our contributions are twofold. Starting with a general image formation model common to most ToF sensors, we draw a striking analogy of ToF systems with sampling theory. Based on our model, we reformulate the ToF super-resolution problem as a parameter estimation problem pivoted around the finite–rate–of–innovation framework. In particular, we show that super–resolution of multi-echo backscattered signal amounts to recovery of Dirac impulses from low-pass measurements. Our theory is corroborated by analysis of data collected from a photon counting, LiDAR sensor, showing the effectiveness of our non-iterative and computationally efficient algorithm.

Index Terms— Finite–rate–of–innovation, multi-path, sampling theory, super–resolution, time–of–flight imaging.

1. INTRODUCTION

In recent years, there has been a surge of research interest in studying time–of–flight or ToF imaging sensors. ToF sensors are active sensors that capture three dimensional information of a scene [5–8]. Unlike conventional digital sensors, a ToF sensor captures two images per acquisition: an amplitude image and a phase/range image. The amplitude image is the usual two dimensional photograph. The unconventional phase image at each pixel provides the depth information of the scene. The range image is computed using the ToF principle—the amount of time it takes for light to reflect back from an object. The amplitude/phase image combination provides a 3D point cloud of the scene.

Several optical ToF systems have been designed [6–8] using either pulsed or continuous wave technology. All these sensors function on the premise that there is a one–to–one mapping between the scene and the sensor. Each sensor pixel is associated with one depth value. In this paper we consider single pixel measurements only, as shown in Fig. 1(a).

In practice, the scene of interest is often complex and results in multi-echo backscattered signal [4,9]. This leads to multiple reflections observed at a given pixel where each reflection (or the corresponding time delay) must be computed to estimate the correct depth value. We discuss this case in Fig. 1(b) and the corresponding LiDAR or *light detection and ranging* based ToF data is plotted in Fig. 1(d). The problem of resolving constituent components of the superimposed echoes has been addressed in a number of papers (cf. [4,9,10] and references therein).

In this paper, we demonstrate *super–resolution* capability using data from a photon counting, ToF imaging sensor. This is a challenging

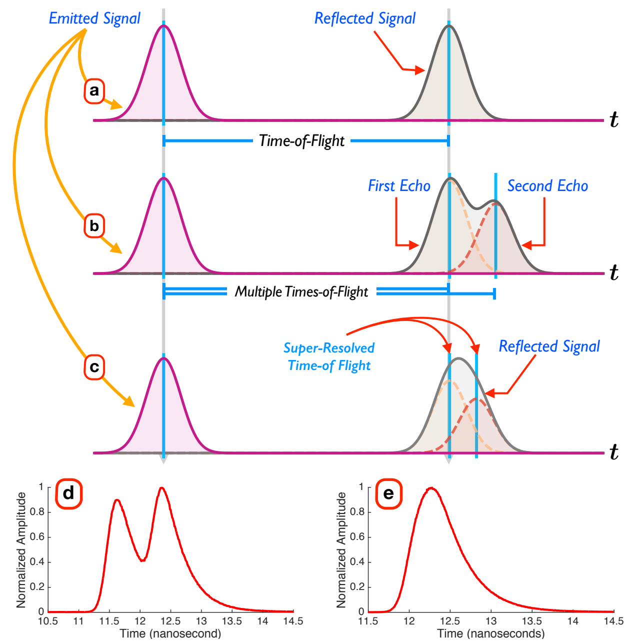

Fig. 1: Illustration of the time–of–flight (ToF) principle. (a) The sensor emits a signal and the reflected signal is time delayed version of the emitted signal. The time delay is proportional to the distance of the object form the sensor. (b) ToF principle in complex environment which suffers from multiple reflected echoes. (c) Challenging case of super-resolution of multiple overlapping echoes. (d) Lidar ToF data corresponding to (b). (e) Lidar ToF data corresponding to the super-resolution problem in (c).

setting in that the backscattered signal contains echoes that defy the *Rayleigh criterion* [11], that is to say, the echoes overlap such that no clear peaks are evident in the return signal. In general, a simple peak finding or correlation algorithm is unable to resolve the two returns. We describe this setting in Fig. 1(c). In 1(e), we plot experimentally acquired LiDAR ToF data.

In previous work [4] et al. have shown how Bayesian analysis of (TCSPC) ToF data can both detect very low signal levels, sometimes less than the background, and also resolve surfaces in depth at the order of 1 cm at a distance of 330 m. In this paper we present a new, non-iterative method to process the ToF data with comparable resolution, thereby allowing deterministic and fixed time processing of lower complexity. We show the comparable performance on the same data set as used previously [4,10].

The remainder of this paper is organized as follows: Starting with a generalized image formation model common to most ToF sensors, we establish a link between ToF sensors and sampling theory [12]. There

Table 1: Different Modalities for Optical Time-of-Flight Sensor Based Depth Imaging

Modality	Probing Function	Reflected Function	IRF	Measurements
CW–ToF(1) [1,2]	$p(t) = 1 + p_0 \cos(\omega_0 t)$		$\varphi(t,\tau) = p(\tau - t)$	$\Gamma_0 \left(1 + \frac{p_0^2}{2} \cos\left(\omega\left(t + \frac{2d_0}{c}\right)\right)\right)$
AMCW–ToF(2) [3]	$p(t) = \text{PN–Sequence}^{(4)}$	$\Gamma_0 p\left(t - \frac{2d_0}{c}\right)$	$\varphi(t,\tau) = p(\tau - t)$	$\Gamma_0 (p * \overline{p})\left(t - \frac{2d_0}{c}\right), \overline{p}(t) = p(-t)$
LIDAR(3) [4]	$p(t) = \delta(t)$		$\varphi(t,\tau) \overset{(8)}{=} \varphi_{\mathbf{\Theta}}(t - \tau)$	$\Gamma_0 \varphi_{\mathbf{\Theta}}(t - 2d_0/c)$

(1) Continuous Wave ToF (2) Amplitude Modulated CW ToF (3) Laser Detection and Ranging (4) Pseudo–random Sequence.

on, we model multiple echoes of light as a sparse signal:

$$h(t) = \sum\nolimits_{k=0}^{K-1} \Gamma_k \delta(t - t_k), \tag{1}$$

where δ denotes Dirac distribution, $\{\Gamma_k\}_{k=0}^{K-1}$ denotes the strength of k^{th} echo and $\{t_k\}_{k=0}^{K-1}$, the corresponding time delay. In summary, we re-formulate the ToF super-resolution problem as recovery of stream of Dirac impulses in (1) from the knowledge of its low-pass filtered samples. Our reinterpretation allows us to invoke the *finite–rate–of–innovation* sampling theory [13, 14]. We demonstrate our results on experiments conducted with LiDAR ToF systems [4, 9]. Compared to previously studied solutions [4, 9], our method enjoys the advantage being non-iterative, of fixed time complexity and faster by capitalizing on spectrum estimation methods [15].

2. TOF IMAGE FORMATION MODEL

2.1. A General Model for ToF Sensors

We begin with a general description of the image formation model for ToF sensors. A ToF system emits a probing function $p(t), t \in \mathbb{R}$ which may be a time-localized pulse or a continuous wave signal. The probing function interacts with the scene or the environment that is characterized by *scene response function* (SRF), $h(t,\tau)$. This results in the reflected signal $r(t)$ modeled by the Fredholm integral operator,

$$p \to \boxed{h} \to \underbrace{r(t) = \int_{\Omega_1} p(\tau)\, h(t,\tau)\, d\tau}_{\text{Reflected Signal}}. \tag{2}$$

The reflected signal is observed at the sensor characterized by *instrument response function* (IRF) or the *sensor response function*, $\varphi(t,\tau)$. For example, in context of optical imaging, this may be thought of as the point spread function. The resulting measurements $m(t)$ then read,

$$r \to \boxed{\varphi} \to \underbrace{m(t) = \int_{\Omega_2} r(\tau)\, \varphi(t,\tau)\, d\tau}_{\text{Measured Signal}}. \tag{3}$$

Finally, the ToF sensor samples the measured signal with the sampling rate Δ and stores a digital sequence, $m[n] = m(t)|_{t=n\Delta}, n \in \mathbb{Z}$.

Based on the choice of probing function, p and the IRF $\varphi(t,\tau)$, ToF imaging modalities may be categorized taxonomically. For example, continuous wave based optical ToF imaging systems [1, 2] such as the Microsoft Kinect use a sinusoidal probing function $p(t) = 1 + \cos(\omega_0 t)$ and the IRF is designed to be $\varphi(t,\tau) = p(\tau - t)$.

In most applications, the SRF is modeled as,

$$h(t,\tau) = \Gamma_0 \delta(t - \tau - 2d_0/c) \tag{4}$$

which leads to a shift–invariant SRF representing a scene at a distance d_0 from the sensor and where $c = 3 \times 10^8$ is the speed of light.

2.2. ToF Sensors and Sampling Theory

In many practical cases of interest, the SRF and the IRF are shift–invariant functions such that,

$$h_{\mathsf{SI}}(t,\tau) = h(t - \tau) \quad \text{and} \quad \varphi_{\mathsf{SI}}(t,\tau) = \varphi(t - \tau), \tag{5}$$

respectively. We list the most prevalent examples in Table 1. Whenever (5) holds, we can rewrite (2) and (3) as convolution integrals and hence,

$$m(t) \overset{(5)}{=} (p * h * \varphi)(t) \equiv (\phi * h)(t), \quad \phi(t) = (p * \varphi)(t). \tag{6}$$

In analogy to shift–invariant *sampling theory* [12], we re-interpret (6), as sampling of an unknown, shift–invariant SRF with sampling kernel ϕ. Finally, the ToF sensor measurements are uniform samples,

$$m[k] = (\phi * h)(t) \sum\nolimits_{k\in\mathbb{Z}} \delta(t - k\Delta). \tag{7}$$

2.3. Lidar Based ToF Imaging

Lidar based imaging sensors probe the scene with a time-localized pulse with resolution of the order of few picoseconds [16] which one may approximate as $p_{\mathsf{LiDAR}}(t) \approx \delta(t)$. Reflection from an opaque surface leads to the SRF in (4) resulting in the reflected signal, $r_{\mathsf{LiDAR}}(t) = \Gamma_0 \delta(t - t_0)$. As shown in [4, 10], the IRF due to SPAD detectors may be modeled as a parametric, shift–invariant kernel of form,

$$\varphi_{\mathbf{\Theta}}(t) = \alpha e^{(a_k - T_0)t + b_k}, \quad t \in I_k \tag{8}$$

where, $\{a_k, b_k\}_{k=1}^{4}$ take 4 different values with continuous transitions, depending whether $t \in I_k$, with $I_1 = (\infty, T_1), I_2 = [T_1, T_2), I_3 = [T_2, T_3), I_4 = (\infty, T_1)$ and $\mathbf{\Theta}$ is an unknown parameter vector,

$$\mathbf{\Theta} = \left[\begin{array}{ccccccccc} \alpha & \sigma & T_0 & T_1 & T_2 & T_3 & \lambda_1 & \lambda_2 & \lambda_3 \end{array}\right]^\top. \tag{9}$$

As a result of this IRF, the measurements read $m(t) = \Gamma_0 \varphi_{\mathbf{\Theta}}(t - t_0)$. As shown in [4, 16], the parameter vector $\mathbf{\Theta}$ may be calibrated and the depth/delay t_0 is estimated using a linear relation [16].

3. SUPER–RESOLVED TOF IMAGING

In this section, we formulate the ToF super-resolution problem. In case when the ToF sensor receives a multi-echo backscattered signal (cf. Fig. 1(b),(c)), the SRF can be modeled as [1, 2, 17],

$$h_{\mathsf{SI}}(t,\tau) = \sum_{k=0}^{K-1} \Gamma_k \delta\left(t - \tau - 2\frac{d_k}{c}\right), \quad c = 3 \times 10^8 \text{ m/s}. \tag{10}$$

In view of (6), the continuous time measurements amount to,

$$m(t) = \sum\nolimits_{k=0}^{K-1} \Gamma_k \phi(t - t_k), \qquad t_k = 2\frac{d_k}{c}. \tag{11}$$

This brings us to our problem statement:

> Given N discrete measurements, $\{m[n]\}_{n=0}^{N-1}$ defined in (7), estimate the SRF in (10) parameterized by $\{\Gamma_k, t_k\}_{k=0}^{K-1}$.

3.1. Bandlimited Approximation of Sampling Kernel

The super-resolution problem is ill–posed if ϕ is unknown. In context of FRI sampling theory, the so–called "sampling kernel" [13, 14] ϕ is assumed to be known. Similarly, in ToF context, ϕ is either designed or calibrated. We discuss two examples based on Table 1.

- In case of AMCW–ToF [1, 2, 18], $p(t)$ is pre-defined and the IRF is the time reversed version of the probing function. Hence,

$$\phi_{\mathsf{AMCW}}(t) = \lim_{T\to\infty} \frac{1}{T}\int_{-T/2}^{+T/2} p(\tau)\, p(t+\tau)\, d\tau \equiv (p * \overline{p})(t), \tag{12}$$

  where $\overline{p}(t) = p(-t)$ denotes the time reversal operation.
- In case of LiDAR based ToF systems, we have $\phi(t) = \varphi_{\boldsymbol{\Theta}}(t)$ (cf. (8)). The parameter vector $\boldsymbol{\Theta}$ is estimated via calibration [4].

In this work, we take an alternate approach towards modeling of ϕ. To this end, we use *bandlimited approximation*, that is, we approximate $\phi(t)$ over an interval of size L with its first M_0 frequency components. This is accomplished by truncating the Fourier series so that,

$$\widetilde{\phi}(t) = \sum_{|m|\leqslant M_0} \widehat{\phi}_m e^{\jmath m\omega_0 t} \quad \text{with} \quad \widehat{\phi}_m = \frac{1}{L}\int_0^L \phi(t)\, e^{-\jmath m\omega_0 t} dt, \tag{13}$$

where $\widetilde{\phi}(t)$ is the M_0–coefficient approximation of $\phi(t)$, $\widehat{\phi}_m, m = -M_0, \ldots, M_0$ are the Fourier Series coefficients of $\phi(t)$ and $\omega_0 = 2\pi/L$ is the fundamental frequency depending on L which is chosen to be the maximum operating range of the ToF system. For example, L may be chosen to be the length of duration of the IRF obtained via calibration. Alternatively, $L = |\max \mathcal{T} - \min \mathcal{T}|, \quad \mathcal{T} = \{t_k\}_{k=0}^{K-1}$.

The bandlimited approximation approach is a natural choice for modeling the sampling kernel ϕ. This is because:

- ♦) Almost all optical systems are approximately bandlimited due to physical limitations. In previous work [18, 19], we have shown that the AMCW ToF (cf. Table 1) based sampling kernel (12) admits a bandlimited approximation. Here, we show the same for LiDAR based systems. Note that $\phi(t) = \varphi_{\boldsymbol{\Theta}}(t)$ (cf. (8)) implying that the sampling kernel is the same as the IRF. In Fig. 2(a), we plot the observed $\phi(t)$ acquired experimentally together with its bandlimited approximation $\widetilde{\phi}$ using $M_0 = 80$.
- ♦) Bandlimited approximation also circumvents the need to estimate the unknown parameter vector $\boldsymbol{\Theta}$ (9) associated with ϕ.

3.2. Super-Resolution via FRI Principles

Bandlimited approximation of ϕ allows us to rewrite (11) as

$$\begin{aligned} m(t) &\stackrel{(11)}{=} \sum_{k=0}^{K-1} \Gamma_k \phi(t-t_k) \\ &\stackrel{(13)}{\approx} \sum_{k=0}^{K-1} \Gamma_k \sum_{|m|\leqslant M_0} \hat{\phi}_m e^{\jmath m\omega_0 (t-t_k)} \\ &= \sum_{|m|\leqslant M_0} \hat{\phi}_m \underbrace{\sum_{k=0}^{K-1} \Gamma_k e^{-\jmath m\omega_0 t_k}}_{y_m} e^{\jmath m\omega_0 t} \\ &= \sum_{|m|\leqslant M_0} \hat{\phi}_m y_m e^{\jmath m\omega_0 t}. \end{aligned} \tag{14}$$

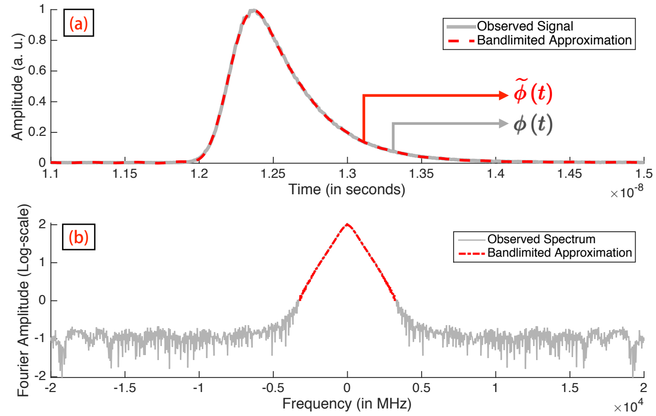

Fig. 2: Instrument response function for LiDAR ToF system. (a) Observed time profile and its Fourier Series approximation (13) with $L = 25$ ns and $M_0 = 80$. (b) Fourier spectrum together with Fourier Series coefficients $\{\widehat{\phi}_m\}_{|m|\leqslant M_0=80}$ (13). With $f_0 = \omega_0/2\pi = 40.0195$ MHz, the maximum frequency used for approximation of $\phi(t)$ is $M_0 f_0$.

In vector–matrix notation we write the sampled measurements (7) as $\mathbf{m} = \mathbf{V}\mathbf{D}_{\Phi}\mathbf{y}$ where,

- $\mathbf{m} \in \mathbb{R}^{N+1}$ is a vector of N, low–pass filtered measurements, $\mathbf{m} \stackrel{(7)}{=} [\ m[0] \ \cdots \ m[N-1]\ ]^{\top}$.
- $\mathbf{V} \in \mathbb{C}^{N\times(2M_0+1)}$ is a Vandermonde/DFT matrix with matrix element $\left[e^{\jmath m\omega_0 n\Delta}\right]_{n,m}$.
- $\mathbf{D}_{\Phi} \in \mathbb{C}^{(2M_0+1)\times(2M_0+1)}$ is a diagonal matrix with matrix element $[\hat{\phi}_m]_{m,m}$ which are the Fourier Series coefficients of ϕ (13).
- $\mathbf{y} \in \mathbb{C}^{(2M_0+1)}$ is a vector of a sum of complex exponentials,
$$y_m = \sum_{k=0}^{K-1} \Gamma_k e^{-\jmath m\omega_0 t_k}. \tag{15}$$

Hence, given $\mathbf{m} = \mathbf{V}\mathbf{D}_{\Phi}\mathbf{y}$, we estimate $\{\Gamma_k, t_k\}_{k=0}^{K-1}$ in two steps:

1. First we obtain the vector $\mathbf{y}$. Provided that $N \geq 2M_0+1$, we have $\mathbf{y} = \mathbf{D}_{\Phi}^{-1}\mathbf{V}^{+}\mathbf{m}$ where $\mathbf{D}_{\Phi}^{-1}$ is the inverted diagonal matrix with elements $[\hat{\phi}_n^{-1}]_{n,n}$ and $(\cdot)^{+}$ denotes the pseudo–inverse operation.
2. Having obtained $\mathbf{y}$, we are left with task of estimating parameters $\{\Gamma_k, t_k\}_{k=0}^{K-1}$. In the noiseless setting, this can be accomplished by using Prony's method which relies on the observation that there exists a sequence $\{h_m\}_{m=0}^{K}$ which *annihilates* y_m [15],
$$y_m + \sum_{l=1}^{K} h_l y_{m-l} = 0, \quad m \geqslant K+1. \tag{16}$$
It turns out that the roots of the polynomial $\mathsf{H}(z)$ constructed with coefficients as $\{h_m\}_{m=0}^{K}$, that is,
$$\mathsf{H}(z) = \prod_{k=0}^{K-1}\left(1 - e^{-\jmath\omega_0 t_k} z^{-1}\right) = \sum_{m=0}^{K-1} h_m z^{-1},$$
encode the information of time delays $\{t_k\}_{k=0}^{K-1}$. This is because $\mathsf{H}\left(e^{-\jmath\omega_0 t_k}\right) = 0$. With $\{t_k\}_{k=0}^{K-1}$, estimating $\{\Gamma_k\}_{k=0}^{K-1}$ boils down to a linear least squares problem,
$$\min_{\{\Gamma_k\}_{k=0}^{K-1}} \sum_{|m|\leqslant M_0} \left| y_m - \sum_{k=0}^{K-1} \Gamma_k e^{-\jmath n\omega_0 t_k} \right|^2.$$

In view of (16), we have $M_0 > K$. With $y_m = y_m^*$, provided that $N \geq K+1$, we can estimate $\{\Gamma_k, t_k\}_{k=0}^{K-1}$ given $\mathbf{m}$. This method can be extended to the *noisy case* [14]. In fact, a number of methods discuss

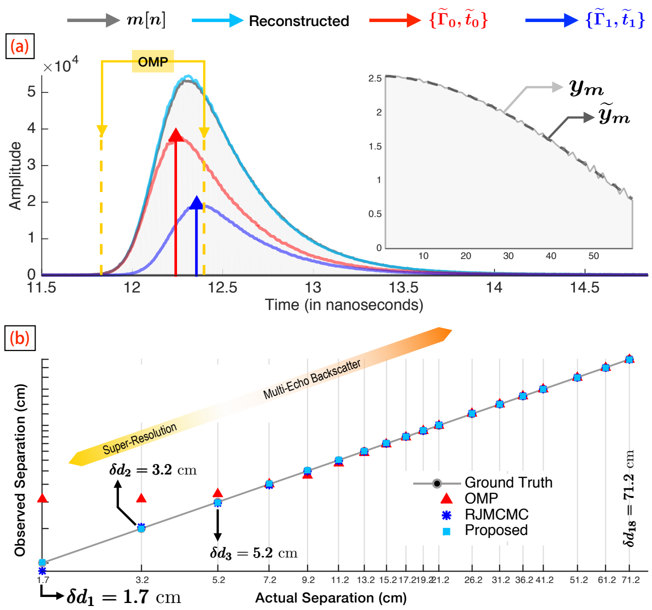

Fig. 3: LiDAR based Super-resolution ToF Imaging. (a) The experiment consists of two retro-reflecting cubes at distance of 330 m from the sensor. We show the recovery of reflectors with inter-reflector separation $\delta d_{\ell_1} = 1.7$ cm. We also plot the result due to Orthogonal Matching Pursuit [21]. (b) We conduct experiments with various separations and plot the results on log–log scale. Our method outperforms previously reported results on the same data in [4].

estimation of $\{\Gamma_k, t_k\}_{k=0}^{K-1}$ given $\mathbf{y}$ in presence on noise. We refer the reader to [15] for a comprehensive overview of techniques. In this work, we will use the *Matrix Pencil Method* due to Hua and Sarkar [20].

3.3. Experimental Results and Performance Evaluation

To measure the depth resolution of the TCSPC-TOF system, two retro-reflecting corner cubes were placed at a distance of 330m from the LiDAR transmitter-receiver and the distance between these surfaces was varied from $\delta d_\ell = 1.7$ cm to 71.2 cm. For a corner cube, all beams, independent of incident angle, are reflected back in the original direction so the behavior is that of a perfect reflecting surface. In these experiments, the timing resolution of the receiver was $\Delta = 6.1$ ps, and the collection time for each histogram was 30s. We calibrated the sampling kernel $\phi(t) = \varphi_{\boldsymbol{\Theta}}(t)$ in (8) which is shown in Fig. 2(a). This is done by recording the response of the LiDAR system to Lambertian reflector.

We plot measurements for $\delta d_1 = 1.7$ cm in Fig. 3(a). Setting $M_0 = 60$ and discarding the boundary values, we use $\mathbf{y} = \mathbf{D}_\Phi^{-1}\mathbf{V}^{+}\mathbf{m}$, to estimate $\{y_m\}_{m=2}^{m=59}$. We then use *Matrix Pencil* method [20] with pencil parameter 1/2 to estimate $\{\widetilde{\Gamma}_k, \widetilde{t}_k\}_{k=0}^{K-1}$. Based on these estimates, we re-synthesize $\{\widetilde{y}_m\}_{m=2}^{m=59}$ using (15) which is plotted in the inset of Fig. 3(a). For the ℓ^{th} experiment with separation δd_ℓ, we estimate the separation using $\widetilde{\delta d_\ell} = 50(\widetilde{t}_2^{(\ell)} - \widetilde{t}_1^{(\ell)})c$ (in cm) with performance metric MSE or the *mean squared error*, $\mathsf{MSE}(\widetilde{\delta d_\ell}, \delta d_\ell) = |50(\widetilde{t}_2^{(\ell)} - \widetilde{t}_1^{(\ell)})c - \delta d_\ell|^2$ as our evaluation metric. The ToF estimates for super-resolution case with $\ell = 1$ results in $[\, \widetilde{t}_1^{(1)}, \widetilde{t}_2^{(1)} \,] = [\, 12.2398, 12.3542 \,]$ ns. Similarly, for $\ell = 2$, we report, $[\, \widetilde{t}_1^{(2)}, \widetilde{t}_2^{(2)} \,] = [\, 12.1338, 12.3474 \,]$ ns. The resulting MSE is,

$$\mathsf{MSE}(\widetilde{\delta d_1}, \delta d_1) = 2.6 \times 10^{-4} \text{ and } \mathsf{MSE}(\widetilde{\delta d_2}, \delta d_2) = 2.5 \times 10^{-5}.$$

respectively. We compare our method to sparse recovery methods such as the OMP or the *Orthogonal Matching Pursuit* [21]. For the super-resolution problem corresponding to $\ell = 1$, the estimates are erroneous, $[\, \widetilde{t}_1^{(1)}, \widetilde{t}_2^{(1)} \,]_{\mathsf{OMP}} = [\, 12.2803, 12.6465 \,]$ with $\mathsf{MSE} = 14.3884$ which is orders of magnitude higher. For higher values of ℓ, the performance of OMP is comparable. We note this behavior for $\ell \geq 3$. RJMCMC based approach of Marin et al. [4] provides better estimates compared to the OMP but is computationally intensive. Our proposed approach provides better estimates compared to OMP and RJMCMC method. For $\{\delta d_\ell\}_{\ell=1}^{18}$ we compare the estimates in Fig. 3(b) and note that our proposed approach is reasonably accurate and outperforms previously reported results on the same data in [4].

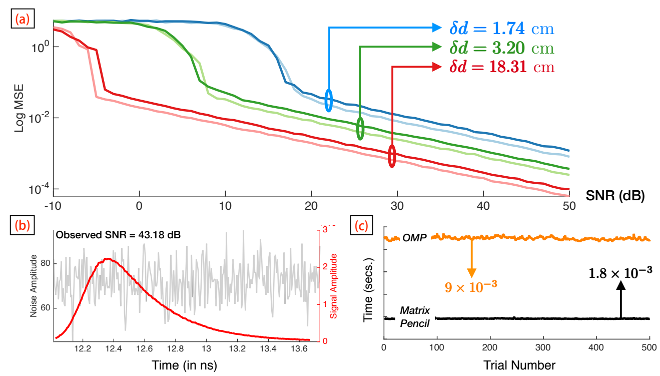

Fig. 4: (a) We setup experiments with separation distances $\delta d = 1.74, 3.20$ and 18.21 cm, respectively and plot the log-MSE as a function of signal–to–noise ratio or the SNR (in dB). (b) We use the IRF to estimate the SNR. The observed SNR for the system is 43.18 dB. (c) We compare computational times for OMP and matrix pencil method. The average of all trials is marked in the figure. In contrast, the RJMCMC method due to [4] requires about a second per pixel.

The matrix pencil method is near optimal in performance (in sense of achieving the Cramér–Rao bounds) [20]. In Fig. 4(a) we plot the MSE as a function of signal–to–noise ratio or the SNR for separations 1.74 cm (super-resolution case), 3.204 cm (super-resolution case) and 18.3105 cm. The performance of our method is consistent with our experiments. We omit discussion on Cramér-Rao bounds in this work due to space limitations but results from [18] may be adapted to our setting. We estimate the system SNR using the IRF which is approximately 43.18 dB (cf. Fig. 4(b)). Furthermore, our method is computationally efficient compared to common-place sparse solver, OMP. As shown in Fig. 4(c), it is about 5 times more efficient. A detailed discussion on computational complexity can be found in [18].

4. CONCLUSION

In this paper, we report a method for super-resolution for ToF signals that is applicable to a wide variety of ToF sensors. We present a unifying image formation model for ToF systems which consolidates two major classes of ToF sensors: AMCW and LiDAR. Based on our image formation model, we draw a parallelism between ToF imaging and sampling theory. In particular, we show that the super-resolution problem in context of ToF imaging can be re-formulated as a finite–rate–of–innovation sampling problem. We discuss the effectivity our approach by performing experiments with LiDAR ToF sensors. Our preliminary experiments show promising results towards super-resolving multi-echo, backscattered, ToF signals. Compared to existing solutions (cf. [4, 9, 10] and references therein), our method is computationally attractive and more accurate in performance.

5. REFERENCES

[1] A. Bhandari, A. Kadambi, R. Whyte, C. Barsi, M. Feigin, A. Dorrington, and R. Raskar, “Resolving multipath interference in time-of-flight imaging via modulation frequency diversity and sparse regularization,” *Optics Letters*, vol. 39, no. 7, 2014.

[2] A. Bhandari, M. Feigin, S. Izadi, C. Rhemann, M. Schmidt, and R. Raskar, “Resolving multipath interference in Kinect: An inverse problem approach,” in *IEEE Sensors*, 2014, pp. 614–617.

[3] B. Büttgen, E. Mechat, M. Hamed-Ali, F. Lustenberger, and P. Seitz, “Pseudonoise optical modulation for real-time 3-D imaging with minimum interference,” *IEEE Trans. on Circuits and Systems I: Regular Papers*, vol. 54, no. 10, pp. 2109–2119, 2007.

[4] S. Hernandez-Marin, A. M. Wallace, and G. J. Gibson, “Bayesian analysis of lidar signals with multiple returns,” *IEEE Transactions on Pattern Analysis and Machine Intelligence*, vol. 29, no. 12, pp. 2170–2180, 2007.

[5] A. Bhandari, S. Izadi, A. Kadambi, R. Raskar, and V. Taamazyan, “Computational 3D imaging: advances in time of flight imaging,” in *ACM SIGGRAPH 2015 Courses*, 2015, p. 8.

[6] J. S. Massa, A. M. Wallace, G. S. Buller, S. J. Fancey, and A. C. Walker, “Laser depth measurement based on time-correlated single-photon counting,” *Optics letters*, vol. 22, no. 8, pp. 543–545, 1997.

[7] S. Foix, G. Alenya, and C. Torras, “Lock-in time-of-flight (ToF) cameras: a survey,” *IEEE Sensors Journal*, vol. 11, no. 9, pp. 1917–1926, 2011.

[8] M. Hansard, S. Lee, O. Choi, and R. P. Horaud, *Time-of-flight cameras: principles, methods and applications*. Springer Science & Business Media, 2012.

[9] C. Mallet, F. Lafarge, M. Roux, U. Soergel, F. Bretar, and C. Heipke, “A marked point process for modeling lidar waveforms,” *IEEE Trans. on Image Processing*, vol. 19, no. 12, pp. 3204–3221, 2010.

[10] G. S. Buller and A. M. Wallace, “Ranging and three-dimensional imaging using time-correlated single-photon counting and point-by-point acquisition,” *IEEE Journal of Selected Topics in Quantum Electronics*, vol. 13, no. 4, pp. 1006–1015, 2007.

[11] J. W. Goodman, *Introduction to Fourier optics*. Roberts and Company Publishers, 2005.

[12] M. Unser, “Sampling–50 years after Shannon,” *Proceedings of the IEEE*, vol. 88, no. 4, pp. 569–587, 2000.

[13] M. Vetterli, P. Marziliano, and T. Blu, “Sampling signals with finite rate of innovation,” *IEEE Transactions on Signal Processing*, vol. 50, no. 6, pp. 1417–1428, 2002.

[14] T. Blu, P.-L. Dragotti, M. Vetterli, P. Marziliano, and L. Coulot, “Sparse sampling of signal innovations,” *IEEE Signal Processing Magazine*, vol. 25, no. 2, pp. 31–40, 2008.

[15] P. Stoica and R. L. Moses, *Introduction to spectral analysis*. Prentice hall Upper Saddle River, 1997, vol. 1.

[16] S. Pellegrini, G. S. Buller, J. M. Smith, A. M. Wallace, and S. Cova, “Laser-based distance measurement using picosecond resolution time-correlated single-photon counting,” *Measurement Science and Technology*, vol. 11, no. 6, p. 712, 2000.

[17] A. Kadambi, R. Whyte, A. Bhandari, L. Streeter, C. Barsi, A. Dorrington, and R. Raskar, “Coded time of flight cameras: sparse deconvolution to address multipath interference and recover time profiles,” *ACM Transactions on Graphics (TOG)*, vol. 32, no. 6, p. 167, 2013.

[18] A. Bhandari, A. Kadambi, and R. Raskar, “Sparse linear operator identification without sparse regularization? Applications to mixed pixel problem in time-of-flight/range imaging,” in *IEEE ICASSP*, 2014, pp. 365–369.

[19] A. Bhandari, C. Barsi, R. Whyte, A. Kadambi, A. J. Das, A. Dorrington, and R. Raskar, “Coded time-of-flight imaging for calibration free fluorescence lifetime estimation,” in *OSA Imaging Systems and Applications*, 2014, pp. IW2C–5.

[20] Y. Hua and T. K. Sarkar, “Matrix pencil method for estimating parameters of exponentially damped/undamped sinusoids in noise,” *IEEE Trans. on Acoustics, Speech and Signal Processing*, vol. 38, no. 5, pp. 814–824, 1990.

[21] Y. C. Pati, R. Rezaiifar, and P. S. Krishnaprasad, “Orthogonal matching pursuit: Recursive function approximation with applications to wavelet decomposition,” in *27 th Asilomar Conf. on Signals, Sys. and Computers*, 1993, pp. 40–44.